Preprints of the 21st IFAC World Congress (Virtual)
Berlin, Germany, July 12-17, 2020

Nonlinear cascade control for a quadrotor transporting a slung load ⋆

Zong-yang Lv * **Yuhu Wu** * **Weiguo xia** * **Wei Wang** *

* *Key Laboratory of Intelligent Control and Optimization for Industrial Equipment of Ministry of Education and School of Control Science and Engineering, Dalian University of Technology, Dalian* 116024*, P. R. China (zongyanglv@mail.dlut.edu.cn, wuyuhu@dlut.edu.cn, wgxiaseu@dlut.edu.cn, wangwei@dlut.edu.cn).*

Abstract: This paper focuses on the motion control problem for a quadrotor with a slung load (QSL). A dynamic model of a QSL is proposed by Lagrangian approach. We considered the air resistance of the load in the model building. Based on such a dynamical model, we propose a novel nonlinear three-loop cascade controller to realize velocity control for the load of a QSL, and the exponential stability of the whole system is proved. Numerical simulations implemented in a Matlab/SimMechanics environment demonstrate the effectiveness of the designed controller and the proposed model.

Keywords: Nonlinear Control, quadrotor, slung load, QSL, exponential stability.

Transporting a load by an unmanned aerial vehicles (UAVs), especially by quadrotors, have been proven useful in many scenarios, such as food delivery, transporting instruments, and manipulate objects for construction, see Choi and Ahn (2015), and Wu et al. (2018b). For the aforementioned cases, one possibility is connecting the load with the quadrotor by a cable. A quadrotor with a slung load (QSL) has been applied for the many advantages, such as weight reduction, loading and unloading the load without landing, and no additional inertia that would reduce the agility of the vehicle Palunko et al. (2012), Sreenath et al. (2013), and Goodarzi et al. (2015). However, in some potential scenarios like Medical supplies and food delivery, the QSL is required to realize stable and accurate transportation, and it's challenging to design a high-performance controller for this system. On the base of quadrotor which is underactuated, the cable and the load form an additional uncontrolled pendulum system, see Qian and Liu (2019). Thus, the system is strongly coupled, nonlinear, and underactuated, and designing a high-performance controller for this system is challenging.

Because of the wide range of applications and challenges of the QSL, some related researches have recently been carried out, in which various control methods are applied to control the QSL. Guerrero et al. (2015b) proposed passivity based control methods to control a QSL, whose aim is to perform path tracking of the quadrotor with loads swing-free. A dynamic programming method by Palunko et al. (2012), and a nonlinear controller by Raffo and de Almeida (2016) have been developed to control the motion of the mass-point load, in which the motion of the load and the quadrotor are measured by camera sensors.

Compared with these works, more practical factors are considered in this paper. In scenarios as fragile instrument transportation, we must consider the velocity of the load to avoid strong shaking in the transportation process. However, if the control law design does not depend on the dynamic of the load as in Guerrero et al. (2015a), strong shaking or collisions may happen in the transportation process. Therefore, a new cascade controller is proposed to control the velocity of the load of a QSL. Furthermore, the exponential stability proof for the entire system is given. Secondly, concerning the problem where the size and weight of the load are usually comparable to the quadrotor, we take the air resistance of the load into account, rather than model the load as a point mass, see Guerrero et al. (2015a), Palunko et al. (2012), and Sreenath et al. (2013).

The main contributions of this paper include: (I) A new model that considers the air resistance of the load is proposed by Lagrangian approach. (II) A novel nonlinear cascade controller is proposed to realize accurate and stable motion control for the load of a QSL, and the exponential stability of the system is proved.

The rest of this paper is organized as follows: In Section II, the dynamical model of a QSL is deduced by Lagrangian approach. In Section III, a nonlinear cascade controller, which consists of three sub-controllers, is proposed. In Section IV, Simulations have been carried out in a SimMechanics environment to evaluate the performance of the controller. Finally, conclusions are given in Section V.

1. DYNAMICAL MODEL OF A QSL

In this section, the dynamical model of a QSL is derived by Lagrangian approach with the following assumptions:
(a) the quadrotor is cross-shaped;
(b) the center of mass of the quadrotor coincides with its body-fixed frame, see Palunko et al. (2012);
(c) the load is fixed on a weightless rigid cable installed on the quadrotor's center by an undamped joint with only 2-dof, and there is no rotational motion around the cable on the payload;
(d) the rotational inertia of the load is relatively small and can be neglected in this work;
(e) QSL works under ideal conditions, where there is no wind disturbance on the QSL.

⋆ This work was supported by the National Natural Science Foundation of China under Grant 61773090 and Grant 61773086 and Liao Ning Revitalization Talents Program under Grant XLYC1907100 and in part by the Fundamental Research Funds for the Central Universities under Grant DUT19LAB37.

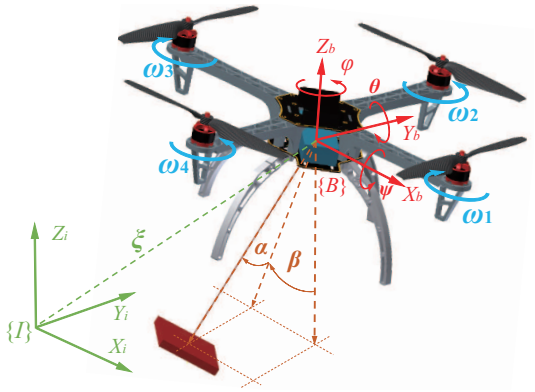

Fig. 1. The structure of QSL.

Fig. 1 shows the structure of a QSL, and two reference frames: the inertial frame $\mathcal{I}\{X_i, Y_i, Z_i\}$ fixed to the ground, the body frame expressed by $\mathcal{B}\{X_b, Y_b, Z_b\}$. Base on the two reference frames, the variables used are described as follows: the generalized coordinates $\boldsymbol{q} = [\boldsymbol{\xi}^\top \ \boldsymbol{\eta}^\top \ \boldsymbol{\sigma}^\top]^\top \in \mathbb{R}^8$, where $\boldsymbol{\xi} = [x \ y \ z]^\top \in \mathbb{R}^3$ are the coordinates of the mass center of the quadrotor in inertial frame $\mathcal{I}$, $\boldsymbol{\eta} = [\phi \ \theta \ \psi]^\top \in \mathbb{R}^3$ are the attitudes of the quadrotor, $\boldsymbol{\sigma} = [\alpha \ \beta]^\top \in \mathbb{R}^2$ are the swing angles of the load in the Euler coordinate system, with the roll angle α and the pitch angle β. $\boldsymbol{\delta} = [x_p \ y_p \ z_p]^\top \in \mathbb{R}^3$ are the coordinates of the mass center of the load in inertial frame $\mathcal{I}$. The boundary of the attitude angles of the load and the quadrotor are limited,

$$\phi, \theta, \alpha, \beta \in (-\pi/2, \pi/2), \psi \in (-\pi, \pi). \tag{1}$$

For convenience, we use $\boldsymbol{s}$ and $\boldsymbol{c}$ to replace sin and cos, $\boldsymbol{0}_{m\times n}$ and $\boldsymbol{E}_n$ to stand for $m \times n$ dimensional null matrix and n-dimensional identity matrix, respectively.

1.1 Lagrangian of a QSL

According to Wu et al. (2018b), the Lagrangian function of the QSL is rewritten in terms of the generalized coordinates $\boldsymbol{q}$,

$$L(\boldsymbol{q}, \dot{\boldsymbol{q}}) = \frac{1}{2}\dot{\boldsymbol{q}}^T \boldsymbol{M}(\boldsymbol{q})\dot{\boldsymbol{q}} - V(\boldsymbol{q}), \tag{2}$$

where the potential energy $V(\boldsymbol{q})$ of the whole QSL is expressed as

$$V(\boldsymbol{q}) = m_q g z + m_p g z_p, \tag{3}$$

with the quadrotor's mass m_q, the load's mass m_p, the gravity acceleration g. Furthermore, the generalized inertia matrix $\boldsymbol{M}(\boldsymbol{q})$ is given by

$$\boldsymbol{M}(\boldsymbol{q}) = \begin{bmatrix} (m_q + m_p)\boldsymbol{E}_3 & \boldsymbol{0}_{3\times 3} & \boldsymbol{M}_2^\top \\ \boldsymbol{0}_{3\times 3} & \boldsymbol{J}_q & \boldsymbol{0}_{3\times 2} \\ \boldsymbol{M}_2 & \boldsymbol{0}_{2\times 3} & \boldsymbol{M}_1 \end{bmatrix}, \tag{4}$$

where $\boldsymbol{J}_q = {\boldsymbol{R}_{eq}^b}^T \boldsymbol{I}_q \boldsymbol{R}_{eq}^b$, $\boldsymbol{R}_{eq}^b \in \mathbb{R}^{3\times 3}$ is the transformation matrix from Euler angular velocity to angular velocity in the body frame, see Arnol'd (2013),

$$\boldsymbol{M}_1 = \mathrm{diag}(m_{77}, m_{88}), \boldsymbol{M}_2 = \begin{bmatrix} m_{71} & m_{72} & m_{73} \\ m_{81} & 0 & m_{83} \end{bmatrix},$$
$$m_{71} = m_p l \boldsymbol{s}\alpha \boldsymbol{s}\beta, \ m_{81} = -m_p l \boldsymbol{c}\alpha \boldsymbol{c}\beta, \ m_{72} = m_p l \boldsymbol{c}\alpha,$$
$$m_{73} = m_p l \boldsymbol{s}\alpha \boldsymbol{c}\beta, \ m_{83} = m_p l \boldsymbol{c}\alpha \boldsymbol{s}\beta, \ m_{77} = m_p l^2 + I_{pxx},$$
$$m_{88} = m_p l^2 \boldsymbol{c}^2\alpha + I_{pyy}\boldsymbol{c}^2\alpha + I_{pzz}\boldsymbol{s}^2\alpha.$$

1.2 Model Derivation for a QSL

The dynamical model of a QSL is described by the *Lagrange – Euler* formulation in Arnol'd (2013),

$$\frac{d}{dt}\frac{\partial L(\boldsymbol{q}, \dot{\boldsymbol{q}})}{\partial \dot{\boldsymbol{q}}} - \frac{\partial L(\boldsymbol{q}, \dot{\boldsymbol{q}})}{\partial \boldsymbol{q}} = \boldsymbol{F}_g. \tag{5}$$

Define general momentum as follows:

$$\boldsymbol{p} = [(\boldsymbol{p}_{\boldsymbol{\xi}} + \boldsymbol{p}_{\boldsymbol{\delta}})^\top \ \ \boldsymbol{p}_{\boldsymbol{\eta}}^\top \ \ \boldsymbol{p}_{\boldsymbol{\sigma}}^\top]^\top \triangleq \partial L(\boldsymbol{q}, \dot{\boldsymbol{q}})/\partial \dot{\boldsymbol{q}}, \tag{6}$$

where

$$\boldsymbol{p}_{\boldsymbol{\xi}} = m_q \dot{\boldsymbol{\xi}}, \ \boldsymbol{p}_{\boldsymbol{\delta}} = m_p \dot{\boldsymbol{\delta}}, \ \boldsymbol{p}_{\boldsymbol{\eta}} = \boldsymbol{J}_q \dot{\boldsymbol{\eta}}, \ \boldsymbol{p}_{\boldsymbol{\sigma}} = \boldsymbol{M}_1 \dot{\boldsymbol{\sigma}} + \boldsymbol{M}_2 \dot{\boldsymbol{\xi}}.$$

From (2), the *Lagrange – Euler* formulation (5) can be expressed as

$$\dot{\boldsymbol{p}} - \partial\left(\dot{\boldsymbol{q}}^\top \boldsymbol{M}(\boldsymbol{q})\dot{\boldsymbol{q}}\right)/\partial 2\boldsymbol{q} + \partial \boldsymbol{V}(\boldsymbol{q})/\partial \boldsymbol{q} = \boldsymbol{F}_g. \tag{7}$$

For (2) and (4), the terms of (7) are given in detail,

$$\partial\left(\dot{\boldsymbol{q}}^\top \boldsymbol{M}(\boldsymbol{q})\dot{\boldsymbol{q}}\right)/\partial 2\boldsymbol{q} = \left[\boldsymbol{0}_{1\times 3} \ \boldsymbol{A}^\top \ \boldsymbol{B}^\top\right]^\top. \tag{8}$$

Furthermore, recalling (3), the derivative of $\boldsymbol{V}(\boldsymbol{q})$ with respect to generalized coordinates $\boldsymbol{q}$ is

$$\partial \boldsymbol{V}(\boldsymbol{q})/\partial \boldsymbol{q} = [\boldsymbol{F}_{qg} + \boldsymbol{F}_{pg} \ \ \boldsymbol{0}_{1\times 3} \ \ \boldsymbol{V}_{d\boldsymbol{\sigma}}]^\top, \tag{9}$$

The external generalized force $\boldsymbol{F}_g$ in (7) is partitioned by the generalized active force $\boldsymbol{F}_a$ and the generalized drag force $\boldsymbol{F}_d$,

$$\boldsymbol{F}_g = \boldsymbol{F}_a + \boldsymbol{F}_d. \tag{10}$$

Here, the generalized active force $\boldsymbol{F}_a$ is given by

$$\boldsymbol{F}_a = \boldsymbol{G}(\boldsymbol{q})\boldsymbol{u},$$

where $\boldsymbol{u} = [F_l \ \ \boldsymbol{\tau}_\eta^\top]^\top$ is the control input of system, which is produced by the thrusts of the rotors, and $\boldsymbol{G} \in \mathbb{R}^{8\times 4}$ is the transfer matrix from the control input $\boldsymbol{u}$ to the generalized active force $\boldsymbol{F}_a$.

The transfer matrix $\boldsymbol{G}$ is given by $\boldsymbol{G}(\boldsymbol{q}) = \begin{bmatrix} \boldsymbol{R} & \boldsymbol{0}_{3\times 3} \\ \boldsymbol{0}_{3\times 1} & \boldsymbol{E}_3 \\ \boldsymbol{0}_{2\times 1} & \boldsymbol{0}_{2\times 3} \end{bmatrix}$, where $\boldsymbol{R} = \boldsymbol{R}_b^i[0 \ 0 \ 1]^\top$ is the projection in the inertial frame $\mathcal{I}$ of the unit vector on the axes Z_b of the body frame $\mathcal{B}$, with the rotation matrix $\boldsymbol{R}_b^i \in \mathbb{R}^{3\times 3}$ from the body frame $\mathcal{B}$ to the inertial frame $\mathcal{I}$, see Arnol'd (2013). In the control input $\boldsymbol{u} = [F_l \ \boldsymbol{\tau}_\eta^\top]^\top$, F_l is the rotors' total thrust, $\boldsymbol{\tau}_\eta = [\tau_\eta \ \tau_\theta \ \tau_\psi]^\top$ is the torque produced by the imbalance of the rotors' thrust. Then, according to Wu et al. (2018a), the control distribution from the four rotors is given as follows,

$$\begin{bmatrix} F_l \\ \tau_\phi \\ \tau_\theta \\ \tau_\psi \end{bmatrix} = \begin{bmatrix} c_t & c_t & c_t & c_t \\ 0 & c_t l_r & 0 & -c_t l_r \\ -c_t l_r & 0 & c_t l_r & 0 \\ -c_q & c_q & -c_q & c_q \end{bmatrix} \begin{bmatrix} \omega_1^2 \\ \omega_2^2 \\ \omega_3^2 \\ \omega_4^2 \end{bmatrix}, \tag{11}$$

where l_r is the distance from the spin axes of the rotors to the center of gravity of the quradrotor, ω_i $(i = 1 \sim 4)$ is the angular velocity of the rotor i, $c_t\omega_i^2$ and $c_q\omega_i^2$ is the thrust and the anti-torque of rotor i, respectively, and the thrust factors c_t and c_q are positive constant, see Davis and Pounds (2017). Then, the generalized active force $\boldsymbol{F}_a$ is rewritten as

$$\boldsymbol{F}_a = [\boldsymbol{R}^\top F_l \ \ \boldsymbol{\tau}_\eta^\top \ \ \boldsymbol{0}_{1\times 2}]^\top. \tag{12}$$

The generalized drag force $\boldsymbol{F}_d$ in (10) is linearized to the general velocities, see Wu et al. (2018b), and given by

$$\boldsymbol{F}_d = [-(\boldsymbol{D}_{\boldsymbol{\xi}}\dot{\boldsymbol{\xi}} + \boldsymbol{D}_{\boldsymbol{\delta}}\dot{\boldsymbol{\delta}})^\top \ \ -(\boldsymbol{D}_{\boldsymbol{\eta}}\dot{\boldsymbol{\eta}})^\top \ \ \boldsymbol{\tau}_{\boldsymbol{\sigma}}^\top]^\top, \tag{13}$$

where $\boldsymbol{D}_{\boldsymbol{\xi}} = \mathrm{diag}(D_{\xi x}, D_{\xi y}, D_{\xi z})$ is the quadrotor's translational drag coefficient matrix, $\boldsymbol{D}_{\boldsymbol{\delta}} = \mathrm{diag}(D_{\delta x}, D_{\delta y}, D_{\delta z})$ denotes the load's translational drag coefficient matrix, $\boldsymbol{D}_{\boldsymbol{\eta}} = \mathrm{diag}(D_\phi, D_\theta, D_\psi)$ denotes the quadrotor's rotational drag torque coefficient matrix. Notice $\boldsymbol{\tau}_{\boldsymbol{\sigma}} = [\tau_\alpha \ \tau_\beta]^\top$ is

the generalized drag torque produced by air resistance and can be calculated as

$$\boldsymbol{\tau_\sigma} = -\boldsymbol{E}_{23}(\boldsymbol{l} \times \boldsymbol{R}_i^{bp} \boldsymbol{D_\delta} \dot{\boldsymbol{\delta}}), \tag{14}$$

where $\boldsymbol{E}_{23} = \begin{bmatrix} 1 & 0 & 0 \\ 0 & 1 & 0 \end{bmatrix}$, $\boldsymbol{l} = [0 \ 0 \ \ -l]^\top$, and $\boldsymbol{R}_i^{bp}$ is the rotational matrix from $\mathcal{I}$ to the load's body frame $\mathcal{B}_p$, according to Arnol'd (2013).

The first three rows of (7) are the transitional dynamics in the inertial frame $\mathcal{I}$ and can be expanded by the first three elements of the forementioned terms (6), (9), (12), and (13),

$$\dot{\boldsymbol{p}}_{\boldsymbol{\xi}} + \dot{\boldsymbol{p}}_\delta + \boldsymbol{F}_{qg} + \boldsymbol{F}_{pg} = \boldsymbol{R} F_l - \boldsymbol{D_\xi} \dot{\boldsymbol{\xi}} - \boldsymbol{D_\delta} \dot{\boldsymbol{\delta}}.$$

According to Newton's second law, the tensile force of the cable on the load is calculated as

$$\boldsymbol{F}_t = \boldsymbol{R} F_l - \dot{\boldsymbol{p}}_{\boldsymbol{\xi}} - \boldsymbol{D_\xi} \dot{\boldsymbol{\xi}} - \boldsymbol{F}_{qg}.$$

Hence, the first three rows of (7) become

$$\dot{\boldsymbol{p}}_{\boldsymbol{\delta}} = \boldsymbol{F}_t - \boldsymbol{D_\delta} \dot{\boldsymbol{\delta}} - \boldsymbol{F}_{pg}. \tag{15}$$

Noting the second three elements of the terms (6), (8), (12), and (13), the middle three rows of (7) are given by

$$\dot{\boldsymbol{p}}_{\boldsymbol{\eta}} - \boldsymbol{A} = \boldsymbol{\tau_\eta} - \boldsymbol{D_\eta} \dot{\boldsymbol{\eta}}. \tag{16}$$

The last two rows of (7) are the rotational dynamics of the swing angles $\boldsymbol{\sigma}$ of the load and are calculated by the last two elements of the terms (6), (8), (9), and (13).

$$\boldsymbol{M}_1 \ddot{\boldsymbol{\sigma}} + \boldsymbol{M}_2 \ddot{\boldsymbol{\xi}} + \dot{\boldsymbol{M}}_1 \dot{\boldsymbol{\sigma}} + \dot{\boldsymbol{M}}_2 \dot{\boldsymbol{\xi}} - \boldsymbol{B} + \boldsymbol{S}_{d\boldsymbol{\sigma}} = \boldsymbol{\tau_\sigma}.$$

Define $\boldsymbol{C} = -\dot{\boldsymbol{M}}_1 \dot{\boldsymbol{\sigma}} - \dot{\boldsymbol{M}}_2 \dot{\boldsymbol{\xi}} + \boldsymbol{B}$. Then, the last two rows of (7) are rewritten as

$$\boldsymbol{M}_1 \ddot{\boldsymbol{\sigma}} = -\boldsymbol{M}_2 \ddot{\boldsymbol{\xi}} - \boldsymbol{S}_{d\boldsymbol{\sigma}} + \boldsymbol{C} + \boldsymbol{\tau_\sigma}. \tag{17}$$

Combining (15), (16) and (17), the dynamic model of the QSL is given as follows:

$$\dot{\boldsymbol{p}}_{\boldsymbol{\delta}} = \boldsymbol{F}_t - \boldsymbol{D_\delta} \dot{\boldsymbol{\delta}} - \boldsymbol{F}_{pg}, \tag{18a}$$

$$\dot{\boldsymbol{p}}_{\boldsymbol{\eta}} = \boldsymbol{\tau_\eta} + \boldsymbol{A} - \boldsymbol{D_\eta} \dot{\boldsymbol{\eta}}, \tag{18b}$$

$$\boldsymbol{M}_1 \ddot{\boldsymbol{\sigma}} = -\boldsymbol{M}_2 \ddot{\boldsymbol{\xi}} - \boldsymbol{S}_{d\boldsymbol{\sigma}} + \boldsymbol{C} + \boldsymbol{\tau_\sigma} \tag{18c}$$

2. DESIGN OF THE NONLINEAR CONTROLLER

In this section, we will design a nonlinear cascade controller for a QSL, which can realize the active velocity control for a load of a QSL and consists of three loops: an inner-loop attitude sub-controller for the quadrotor, a middle-loop swing angle sub-controller for the load, and the outer-loop velocity sub-controller for the load. The main objective of the controller is to guarantee that the velocity $\dot{\boldsymbol{\delta}}$ of the load can track the desired velocity $\dot{\boldsymbol{\delta}}_d$. The schematic of the controller is shown in Fig. 2.

2.1 Tracking Errors

A specific errors model will be introduced for the following controller design and stability analysis. The tracking errors for $\dot{\boldsymbol{\delta}}$, $\boldsymbol{\sigma}$, $\boldsymbol{\eta}$ and the corresponding $\ddot{\boldsymbol{\delta}}$, $\boldsymbol{p_\sigma}$, $\boldsymbol{p_\eta}$ will be given.

Define

$$\boldsymbol{e}_{\boldsymbol{\eta},\boldsymbol{p_\eta}} = [\boldsymbol{e}_{\boldsymbol{\eta}}^\top \ \boldsymbol{e}_{\boldsymbol{p_\eta}}^\top]^\top, \tag{19}$$

where $\boldsymbol{e_\eta} = \boldsymbol{\eta}_d - \boldsymbol{\eta}$, $\boldsymbol{e}_{\boldsymbol{p_\eta}} = \dot{\boldsymbol{\eta}}_d - \dot{\boldsymbol{\eta}} + \boldsymbol{K_\eta} \boldsymbol{e_\eta}$, with the desired attitude $\boldsymbol{\eta}_d$, the desired Euler angular velocity $\dot{\boldsymbol{\eta}}_d$, and is positive definite matrix $\boldsymbol{K_\eta} = \mathrm{diag}(k_1, k_2, k_3)$. Then we can obtain the following attitude error dynamic,

$$\dot{\boldsymbol{e}}_{\boldsymbol{\eta}} = \boldsymbol{e}_{\boldsymbol{p_\eta}} - \boldsymbol{K_\eta} \boldsymbol{e_\eta}, \ \dot{\boldsymbol{e}}_{\boldsymbol{p_\eta}} = \ddot{\boldsymbol{\eta}}_d - \ddot{\boldsymbol{\eta}} + \boldsymbol{K_\eta} (\boldsymbol{e}_{\boldsymbol{p_\eta}} - \boldsymbol{K_\eta} \boldsymbol{e_\eta}). \tag{20}$$

Define

$$\boldsymbol{e}_{\boldsymbol{\sigma},\boldsymbol{p_\sigma}} = [\boldsymbol{e}_{\boldsymbol{\sigma}}^\top \ \boldsymbol{e}_{\boldsymbol{p_\sigma}}^\top]^\top, \tag{21}$$

where $\boldsymbol{e_\sigma} = [e_\alpha \ e_\beta]^\top = \boldsymbol{\sigma}_d - \boldsymbol{\sigma}$, $\boldsymbol{e}_{\boldsymbol{p_\sigma}} = \dot{\boldsymbol{\sigma}}_d - \dot{\boldsymbol{\sigma}} + \boldsymbol{K_\sigma} \boldsymbol{e_\sigma}$, with the desired swing angle $\boldsymbol{\sigma}_d$, the desired swing velocity $\dot{\boldsymbol{\sigma}}_d$, and positive definite matrix $\boldsymbol{K_\sigma} = \mathrm{diag}(k_7, k_8)$. The attitude error dynamic is obtained as follows,

$$\dot{\boldsymbol{e}}_{\boldsymbol{\sigma}} = \boldsymbol{e}_{\boldsymbol{p_\sigma}} - \boldsymbol{K_\sigma} \boldsymbol{e_\sigma}, \ \dot{\boldsymbol{e}}_{\boldsymbol{p_\sigma}} = \ddot{\boldsymbol{\sigma}}_d - \ddot{\boldsymbol{\sigma}} + \boldsymbol{K_\sigma} (\boldsymbol{e}_{\boldsymbol{p_\sigma}} - \boldsymbol{K_\sigma} \boldsymbol{e_\sigma}). \tag{22}$$

Define

$$\boldsymbol{e}_{\dot{\boldsymbol{\delta}}} = \dot{\boldsymbol{\delta}}_d - \dot{\boldsymbol{\delta}}, \ \boldsymbol{e}_{\ddot{\boldsymbol{\delta}}} = \dot{\boldsymbol{e}}_{\dot{\boldsymbol{\delta}}} = \ddot{\boldsymbol{\delta}}_d - \ddot{\boldsymbol{\delta}}, \tag{23}$$

where $\dot{\boldsymbol{\delta}}_d$ is the desired velocity of the load and $\ddot{\boldsymbol{\delta}}_d$ is the corresponding desired acceleration of the load.

2.2 Cascade Nonlinear Controller

For the subsystems (18b), the inner-loop attitude sub-controller, as illustrated in the inner-loop part of the Fig. (2), is used to control the quadrotor's attitude $\boldsymbol{\eta}$ and stabilize it to avoid strong shaking or crashing, which is realized by the torque $\boldsymbol{\tau_\eta}$ produced by the imbalance of the thrust of rotors. The torque $\boldsymbol{\tau_\eta}$ is chosen as

$$\boldsymbol{\tau_\eta} = \boldsymbol{J}_q (\boldsymbol{e_\eta} + \boldsymbol{K_\eta} \boldsymbol{e}_{\boldsymbol{p_\eta}} - \boldsymbol{K}_{\boldsymbol{\eta}}^2 \boldsymbol{e_\eta} + \boldsymbol{K}_{\boldsymbol{p_\eta}} \boldsymbol{e}_{\boldsymbol{p_\eta}}) + \dot{\boldsymbol{J}}_{\boldsymbol{q}} \dot{\boldsymbol{\eta}} - \boldsymbol{A} + \boldsymbol{D_\eta} \dot{\boldsymbol{\eta}}, \tag{24}$$

where $\boldsymbol{K}_{\boldsymbol{p_\eta}} = \mathrm{diag}(k_4, k_5, k_6)$ are positive definite.

Considering the subsystems (18c), the middle-loop swing angle sub-controller, as illustrated in the middle-loop part of the Fig. (2), is applied to control the swing angle $\boldsymbol{\sigma}$ of the load and the tensile force F_t , and includes two parts: a swing angle controller and a decoupler. In the middle-loop sub-controller, for a desired swing angle $\boldsymbol{\sigma}_d$, the swing angular acceleration $\ddot{\boldsymbol{\sigma}}$ is chosen as

$$\ddot{\boldsymbol{\sigma}}_v = (\boldsymbol{E}_2 - \boldsymbol{K}_{\boldsymbol{\sigma}}^2) \boldsymbol{e_\sigma} + (\boldsymbol{K_\sigma} + \boldsymbol{K}_{\boldsymbol{p_\sigma}}) \boldsymbol{e}_{\boldsymbol{p_\sigma}}, \tag{25}$$

where, $\boldsymbol{K}_{\boldsymbol{p_\sigma}} = \mathrm{diag}(k_9, k_{10})$ are positive definite.

In the decoupler, we will decouple the F_l, ϕ_d and θ_d from F_{td} and $\ddot{\boldsymbol{\sigma}}_v$. As the inextensibility of the rigid cable, the quadrotor and the load have the same translational acceleration along the direction of the cable. Thus, combining (18c), we can get the the following equations,

$$F_{td} = [0 \ 0 \ 1] \boldsymbol{R}_i^{bp} [\ddot{\boldsymbol{\xi}}_d + (\boldsymbol{D_\delta} \dot{\boldsymbol{\delta}} + \boldsymbol{F}_{pg})/m_p], \tag{26a}$$

$$\boldsymbol{M}_1 \ddot{\boldsymbol{\sigma}}_v = -\boldsymbol{M}_2 \ddot{\boldsymbol{\xi}}_d - \boldsymbol{S}_{d\boldsymbol{\sigma}} + \boldsymbol{C} + \boldsymbol{\tau_\sigma}. \tag{26b}$$

From (26), we can solve for $\ddot{\boldsymbol{\xi}}_d$ by F_{td} and $\ddot{\boldsymbol{\sigma}}_v$. The desired lift force is expressed by $\boldsymbol{F}_{ld}$ in the inertial frame, which is coupled with the desired translational acceleration of the load $\ddot{\boldsymbol{\xi}}_d$. The quadrotor is driven by the lift force $\boldsymbol{F}_l$, the tensile force $-\boldsymbol{R}_i^{bp\top} [0 \ 0 \ F_t]^\top$, the gravity force $\boldsymbol{F}_{qg}$, and the drag force $\boldsymbol{D_\xi} \dot{\boldsymbol{\xi}}$. Thus,

$$\boldsymbol{F}_{ld} = m_q \ddot{\boldsymbol{\xi}}_d + \boldsymbol{R}_i^{bp\top} [0 \ 0 \ F_{td}]^\top + \boldsymbol{F}_{qg} + \boldsymbol{D_\xi} \dot{\boldsymbol{\xi}}. \tag{27}$$

The total thrust F_l of the rotors and the desired swing angles ϕ_d, θ_d is obtained by decoupling the desired lift force $\boldsymbol{F}_{ld}$, the transformation is given by

$$\begin{bmatrix} \boldsymbol{c}\psi & -\boldsymbol{s}\psi & 0 \\ \boldsymbol{s}\psi & \boldsymbol{c}\psi & 0 \\ 0 & 0 & 1 \end{bmatrix} \begin{bmatrix} \boldsymbol{c}\theta_d & 0 & \boldsymbol{s}\theta_d \\ 0 & 1 & 0 \\ -\boldsymbol{s}\theta_d & 0 & \boldsymbol{c}\theta_d \end{bmatrix} \begin{bmatrix} 1 & 0 & 0 \\ 0 & \boldsymbol{c}\phi_d & -\boldsymbol{s}\phi_d \\ 0 & \boldsymbol{s}\phi_d & \boldsymbol{c}\phi_d \end{bmatrix} \begin{bmatrix} 0 \\ 0 \\ F_l \end{bmatrix} = \boldsymbol{F}_{ld}. \tag{28}$$

Solving (28),

$$\theta_d = arctan\left((F_{lxd} \boldsymbol{c}\psi + F_{lyd} \boldsymbol{s}\psi)/F_{lzd}\right), \tag{29a}$$

$$\phi_d = -\ arctan\left((-F_{lxd} \boldsymbol{s}\psi + F_{lyd} \boldsymbol{c}\psi) \boldsymbol{c}\theta_d / F_{lzd}\right), \tag{29b}$$

$$F_l = F_{lzd}/(\boldsymbol{c}\phi_d \boldsymbol{c}\theta_d). \tag{29c}$$

For subsystems (18a), the outer-loop controller, as illustrated in the Fig. (2), is applied to guarantee the load's velocity $\dot{\boldsymbol{\delta}}$ can follow the desired velocity $\dot{\boldsymbol{\delta}}_d$, which is

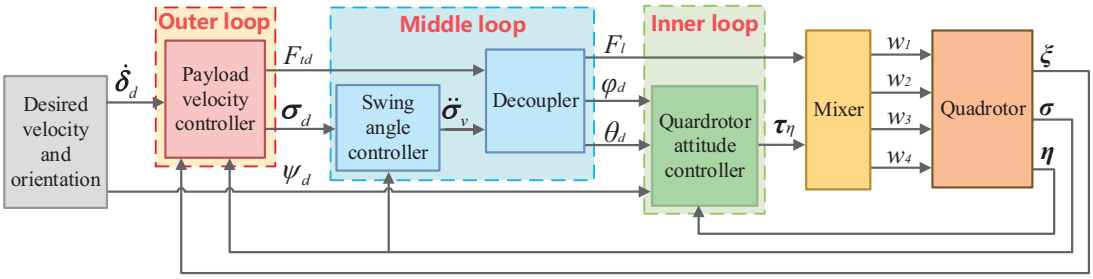

Fig. 2. The schematic of the nonlinear controller for QSL

realized by the desired tensile force $\boldsymbol{F}_{td} = [F_{txd}\ F_{tyd}\ F_{tzd}]^\top$ on the cable. Like (29), The magnitude of the desired tensile force $\boldsymbol{F}_{td}$ and the desired swing angles α_d and β_d are given by

$$F_{td} = F_{tzd}/(\boldsymbol{c}\alpha_d \boldsymbol{c}\theta_d), \tag{30a}$$
$$\beta_d = arctan(F_{txd}/F_{tzd}), \tag{30b}$$
$$\alpha_d = -arctan(F_{tyd}/(F_{tzd}\boldsymbol{c}\beta_d)), \tag{30c}$$

where

$$\boldsymbol{F}_{td} = \boldsymbol{K}_{\dot{\boldsymbol{\delta}}}\boldsymbol{e}_{\dot{\boldsymbol{\delta}}} + \boldsymbol{F}_{pg} + \boldsymbol{D}_{\boldsymbol{\delta}}\dot{\boldsymbol{\delta}}, \tag{31}$$

with positive definite matrixes $\boldsymbol{K}_{\dot{\boldsymbol{\delta}}} = \mathrm{diag}(k_{11}, k_{12}, k_{13})$ and $\boldsymbol{K}_{\ddot{\boldsymbol{\sigma}}} = \mathrm{diag}(k_{14}, k_{15}, k_{16})$.

2.3 Stability Analysis of the Entire Cascade Controller

In this subsection, we construct a special Lyapunov candidate to prove the exponential stability of the entire system.

Theorem 1. For the dynamical model of the QSL defined in (18), with a fixed desired reference velocity $\dot{\boldsymbol{\delta}}_d$ with $\ddot{\boldsymbol{\delta}}_d = 0$. If the entire cascade controller (24), (25) and (28) has been applied to control the QSL, the zero equilibrium of the errors $\boldsymbol{e}_{\dot{\boldsymbol{\delta}}}$, $\boldsymbol{e}_{\boldsymbol{\sigma},\boldsymbol{p}_\sigma}$ and $\boldsymbol{e}_{\boldsymbol{\eta},\boldsymbol{p}_\eta}$ are exponentially stable.

Proof. The Lyapunov candidate $V_t(\boldsymbol{e}_{\dot{\boldsymbol{\delta}}}, \boldsymbol{e}_{\boldsymbol{\sigma},\boldsymbol{p}_\sigma}, \boldsymbol{e}_{\boldsymbol{\eta},\boldsymbol{p}_\eta})$ is defined to check the stability of the entire designed controller,

$$V_t(\boldsymbol{e}_{\dot{\boldsymbol{\delta}}}, \boldsymbol{e}_{\boldsymbol{\sigma},\boldsymbol{p}_\sigma}, \boldsymbol{e}_{\boldsymbol{\eta},\boldsymbol{p}_\eta}) = aV_{\dot{\boldsymbol{\delta}}}(\boldsymbol{e}_{\dot{\boldsymbol{\delta}}}) + bV_{\boldsymbol{\sigma}}(\boldsymbol{e}_{\boldsymbol{\sigma},\boldsymbol{p}_\sigma}) + \sqrt{V_{\boldsymbol{\eta}}(\boldsymbol{e}_{\boldsymbol{\eta},\boldsymbol{p}_\eta})}, \tag{32}$$

where $V_{\dot{\boldsymbol{\delta}}}(\boldsymbol{e}_{\dot{\boldsymbol{\delta}}}) = \frac{1}{2}\|\boldsymbol{e}_{\dot{\boldsymbol{\delta}}}\|^2$, $V_{\boldsymbol{\sigma}}(\boldsymbol{e}_{\boldsymbol{\sigma},\boldsymbol{p}_\sigma}) = \frac{1}{2}\|\boldsymbol{e}_{\boldsymbol{\sigma},\boldsymbol{p}_\sigma}\|^2$, $V_{\boldsymbol{\eta}}(\boldsymbol{e}_{\boldsymbol{\eta},\boldsymbol{p}_\eta}) = \frac{1}{2}\|\boldsymbol{e}_{\boldsymbol{\eta},\boldsymbol{p}_\eta}\|^2$,

$$b < \lambda_{\boldsymbol{\eta}}/L_2,\ a < 4bm_p^2\lambda_{\dot{\boldsymbol{\delta}}}\lambda_{\boldsymbol{\sigma}}/L_1^2, \tag{33}$$

with $\lambda_{\boldsymbol{\eta}}$, $\lambda_{\dot{\boldsymbol{\delta}}}$ and $\lambda_{\boldsymbol{\sigma}}$ is defined in (42).

The time derivative of V_t in (32) is

$$\begin{aligned}\dot{V}_t =& a\frac{\partial V_{\dot{\boldsymbol{\delta}}}}{\partial \boldsymbol{e}_{\dot{\boldsymbol{\delta}}}}\dot{\boldsymbol{e}}_{\dot{\boldsymbol{\delta}}}(\boldsymbol{e}_{\dot{\boldsymbol{\delta}}}, \boldsymbol{e}_{\boldsymbol{F}_t}) + b\frac{\partial V_{\boldsymbol{\sigma}}}{\partial \boldsymbol{e}_{\boldsymbol{\sigma},\boldsymbol{p}_\sigma}}\dot{\boldsymbol{e}}_{\boldsymbol{\sigma},\boldsymbol{p}_\sigma}(\boldsymbol{e}_{\boldsymbol{\sigma},\boldsymbol{p}_\sigma}, \boldsymbol{e}_{\ddot{\boldsymbol{\sigma}}}) + \frac{\dot{V}_{\boldsymbol{\eta}}}{2\sqrt{V_{\boldsymbol{\eta}}}} \\ =& a\frac{\partial V_{\dot{\boldsymbol{\delta}}}}{\partial \boldsymbol{e}_{\dot{\boldsymbol{\delta}}}}\dot{\boldsymbol{e}}_{\dot{\boldsymbol{\delta}}}(\boldsymbol{e}_{\dot{\boldsymbol{\delta}}}, 0) + a\frac{\partial V_{\dot{\boldsymbol{\delta}}}}{\partial \boldsymbol{e}_{\dot{\boldsymbol{\delta}}}}[\dot{\boldsymbol{e}}_{\dot{\boldsymbol{\delta}}}(\boldsymbol{e}_{\dot{\boldsymbol{\delta}}}, \boldsymbol{e}_{\boldsymbol{F}_t}) - \dot{\boldsymbol{e}}_{\dot{\boldsymbol{\delta}}}(\boldsymbol{e}_{\dot{\boldsymbol{\delta}}}, 0)] \\ &+ b\frac{\partial V_{\boldsymbol{\sigma}}}{\partial \boldsymbol{e}_{\boldsymbol{\sigma},\boldsymbol{p}_\sigma}}\dot{\boldsymbol{e}}_{\boldsymbol{\sigma},\boldsymbol{p}_\sigma}(\boldsymbol{e}_{\boldsymbol{\sigma},\boldsymbol{p}_\sigma}, 0) + b\frac{\partial V_{\boldsymbol{\sigma}}}{\partial \boldsymbol{e}_{\boldsymbol{\sigma},\boldsymbol{p}_\sigma}}[\dot{\boldsymbol{e}}_{\boldsymbol{\sigma},\boldsymbol{p}_\sigma}(\boldsymbol{e}_{\boldsymbol{\sigma},\boldsymbol{p}_\sigma}, \boldsymbol{e}_{\ddot{\boldsymbol{\sigma}}}) \\ &- \dot{\boldsymbol{e}}_{\boldsymbol{\sigma},\boldsymbol{p}_\sigma}(\boldsymbol{e}_{\boldsymbol{\sigma},\boldsymbol{p}_\sigma}, 0)] + \boldsymbol{e}_{\boldsymbol{\eta},\boldsymbol{p}_\eta}^\top\dot{\boldsymbol{e}}_{\boldsymbol{\eta},\boldsymbol{p}_\eta}/(\sqrt{2}\|\boldsymbol{e}_{\boldsymbol{\eta},\boldsymbol{p}_\eta}\|).\end{aligned} \tag{34}$$

Noting (18a), and $\ddot{\boldsymbol{\delta}}_d = 0$, the time derivative of $\boldsymbol{e}_{\dot{\boldsymbol{\delta}}}$ is

$$\dot{\boldsymbol{e}}_{\dot{\boldsymbol{\delta}}} = -m_p^{-1}(\boldsymbol{F}_t - \boldsymbol{D}_{\boldsymbol{\delta}}\dot{\boldsymbol{\delta}} - \boldsymbol{F}_{pg}). \tag{35}$$

Define

$$\boldsymbol{e}_{\boldsymbol{F}_t} = \boldsymbol{F}_{td} - \boldsymbol{F}_t, \tag{36}$$

then, (35) becomes $\dot{\boldsymbol{e}}_{\dot{\boldsymbol{\delta}}} = -m_p^{-1}(\boldsymbol{F}_{td} - \boldsymbol{e}_{\boldsymbol{F}\boldsymbol{t}} - \boldsymbol{D}_{\boldsymbol{\delta}}\dot{\boldsymbol{\delta}} - \boldsymbol{F}_{pg})$. By (31), this equation becomes

$$\dot{\boldsymbol{e}}_{\dot{\boldsymbol{\delta}}}(\boldsymbol{e}_{\dot{\boldsymbol{\delta}}}, \boldsymbol{e}_{\boldsymbol{F}\boldsymbol{t}}) = m_p^{-1}(\boldsymbol{e}_{\boldsymbol{F}\boldsymbol{t}} - \boldsymbol{K}_{\dot{\boldsymbol{\delta}}}\boldsymbol{e}_{\dot{\boldsymbol{\delta}}}). \tag{37}$$

As $\dot{\boldsymbol{\sigma}}_d$ is constant, $\ddot{\boldsymbol{\sigma}}_d = 0$. Noticing $\dot{\boldsymbol{e}}_{\boldsymbol{\sigma}}$, $\boldsymbol{e}_{\boldsymbol{\sigma},\boldsymbol{p}_\sigma} = [\boldsymbol{e}_{\boldsymbol{\sigma}}^\top\ \boldsymbol{e}_{\boldsymbol{p}_\sigma}^\top]^\top$ in (21) is $\dot{\boldsymbol{e}}_{\boldsymbol{\sigma},\boldsymbol{p}_\sigma} = \begin{bmatrix} \boldsymbol{e}_{\boldsymbol{p}_\sigma} - \boldsymbol{K}_{\boldsymbol{\sigma}}\boldsymbol{e}_{\boldsymbol{\sigma}} \\ -\ddot{\boldsymbol{\sigma}} + \boldsymbol{K}_{\boldsymbol{\sigma}}(\boldsymbol{e}_{\boldsymbol{p}_\sigma} - \boldsymbol{K}_{\boldsymbol{\sigma}}\boldsymbol{e}_{\boldsymbol{\sigma}}) \end{bmatrix}$. Define $\boldsymbol{e}_{\ddot{\boldsymbol{\sigma}}} = \ddot{\boldsymbol{\sigma}}_v - \ddot{\boldsymbol{\sigma}}$, where $\ddot{\boldsymbol{\sigma}}_v$ is given in (25). Substituting $\boldsymbol{e}_{\ddot{\boldsymbol{\sigma}}}$ into $\dot{\boldsymbol{e}}_{\boldsymbol{\sigma},\boldsymbol{p}_\sigma}$, we obtain

$$\dot{\boldsymbol{e}}_{\boldsymbol{\sigma},\boldsymbol{p}_\sigma}(\boldsymbol{e}_{\boldsymbol{\sigma},\boldsymbol{p}_\sigma}, \boldsymbol{e}_{\ddot{\boldsymbol{\sigma}}}) = \begin{bmatrix} \boldsymbol{e}_{\boldsymbol{p}_\sigma} - \boldsymbol{K}_{\boldsymbol{\sigma}}\boldsymbol{e}_{\boldsymbol{\sigma}} \\ \boldsymbol{e}_{\ddot{\boldsymbol{\sigma}}} - \boldsymbol{e}_{\boldsymbol{\sigma}} - \boldsymbol{K}_{\boldsymbol{p}_\sigma}\boldsymbol{e}_{\boldsymbol{p}_\sigma} \end{bmatrix}. \tag{38}$$

Since the desired angular velocity $\dot{\boldsymbol{\eta}}_d$ is constant, its derivative $\ddot{\boldsymbol{\eta}}_d = 0$. Considering $\dot{\boldsymbol{e}}_{\boldsymbol{\eta}}$ and $\dot{\boldsymbol{e}}_{\boldsymbol{p}_\eta}$ in (20), the time derivative of $\boldsymbol{e}_{\boldsymbol{\eta},\boldsymbol{p}_\eta} = [\boldsymbol{e}_{\boldsymbol{\eta}}^\top\ \boldsymbol{e}_{\boldsymbol{p}_\eta}^\top]^\top$ in (19) is $\dot{\boldsymbol{e}}_{\boldsymbol{\eta},\boldsymbol{p}_\eta} = \begin{bmatrix} \boldsymbol{e}_{\boldsymbol{p}_\eta} - \boldsymbol{K}_{\boldsymbol{\eta}}\boldsymbol{e}_{\boldsymbol{\eta}} \\ -\ddot{\boldsymbol{\eta}} + \boldsymbol{K}_{\boldsymbol{\eta}}(\boldsymbol{e}_{\boldsymbol{p}_\eta} - \boldsymbol{K}_{\boldsymbol{\eta}}\boldsymbol{e}_{\boldsymbol{\eta}}) \end{bmatrix}$. Substituting (18b) into former equation and choosing the desired torque $\boldsymbol{\tau}_{\boldsymbol{\eta}}$ in (24), we get $\dot{\boldsymbol{e}}_{\boldsymbol{\eta},\boldsymbol{p}_\eta} = \begin{bmatrix} \boldsymbol{e}_{\boldsymbol{p}_\eta} - \boldsymbol{K}_{\boldsymbol{\eta}}\boldsymbol{e}_{\boldsymbol{\eta}} \\ -\boldsymbol{e}_{\boldsymbol{\eta}} - \boldsymbol{K}_{\boldsymbol{p}_\eta}\boldsymbol{e}_{\boldsymbol{p}_\eta} \end{bmatrix}$.

Substituting (37), (38), and above equation into (34) yields

$$\begin{aligned}\dot{V}_t =& -am_p^{-1}\boldsymbol{e}_{\dot{\boldsymbol{\delta}}}\boldsymbol{K}_{\dot{\boldsymbol{\delta}}}\boldsymbol{e}_{\dot{\boldsymbol{\delta}}} + am_p^{-1}\|\boldsymbol{e}_{\dot{\boldsymbol{\delta}}}\|(\dot{\boldsymbol{e}}_{\dot{\boldsymbol{\delta}}}(\boldsymbol{e}_{\dot{\boldsymbol{\delta}}}, \boldsymbol{e}_{\boldsymbol{F}_t}) - \dot{\boldsymbol{e}}_{\dot{\boldsymbol{\delta}}}(\boldsymbol{e}_{\dot{\boldsymbol{\delta}}}, 0)) \\ &+ b\boldsymbol{e}_{\boldsymbol{\sigma}}^\top(\boldsymbol{e}_{\boldsymbol{p}_\sigma} - \boldsymbol{K}_{\boldsymbol{\sigma}}\boldsymbol{e}_{\boldsymbol{\sigma}}) - b\boldsymbol{e}_{\boldsymbol{p}_\sigma}^\top(\boldsymbol{e}_{\boldsymbol{\sigma}} + \boldsymbol{K}_{\boldsymbol{p}_\sigma}\boldsymbol{e}_{\boldsymbol{p}_\sigma}) \\ &+ b\partial V_{\boldsymbol{\sigma}}/\partial \boldsymbol{e}_{\boldsymbol{\sigma},\boldsymbol{p}_\sigma}[\dot{\boldsymbol{e}}_{\boldsymbol{\sigma},\boldsymbol{p}_\sigma}(\boldsymbol{e}_{\boldsymbol{\sigma},\boldsymbol{p}_\sigma}, \boldsymbol{e}_{\ddot{\boldsymbol{\sigma}}}) - \dot{\boldsymbol{e}}_{\boldsymbol{\sigma},\boldsymbol{p}_\sigma}(\boldsymbol{e}_{\boldsymbol{\sigma},\boldsymbol{p}_\sigma}, 0)] \\ &- (\boldsymbol{e}_{\boldsymbol{\eta}}^\top\boldsymbol{K}_{\boldsymbol{\eta}}\boldsymbol{e}_{\boldsymbol{\eta}} + \boldsymbol{e}_{\boldsymbol{p}_\eta}^\top\boldsymbol{K}_{\boldsymbol{p}_\eta}\boldsymbol{e}_{\boldsymbol{p}_\eta})/(\sqrt{2}\|\boldsymbol{e}_{\boldsymbol{\eta},\boldsymbol{p}_\eta}\|).\end{aligned} \tag{39}$$

According to (37), $\dot{\boldsymbol{e}}_{\dot{\boldsymbol{\delta}}}$ is Lipschitz with respect to $\boldsymbol{e}_{F_t}$. For (30), $\boldsymbol{e}_{\boldsymbol{F}_t}$ in (36) can be expressed as $\boldsymbol{e}_{\boldsymbol{F}_t}(\boldsymbol{e}_{\boldsymbol{\sigma}}, \boldsymbol{e}_{F_t})$, where $\boldsymbol{e}_{F_t} = 0$ as F_t can always track F_{td}, so $\boldsymbol{e}_{\boldsymbol{F}_t}(\boldsymbol{e}_{\boldsymbol{\sigma}}, \boldsymbol{e}_{F_t})$ is rewritten as $\boldsymbol{e}_{\boldsymbol{F}_t}(\boldsymbol{e}_{\boldsymbol{\sigma}})$. It is easy to prove that $\boldsymbol{e}_{\boldsymbol{F}_t}(\boldsymbol{e}_{\boldsymbol{\sigma}})$ is Lipschitz with respect to $\boldsymbol{e}_{\boldsymbol{\sigma}}$. Thus, $\dot{\boldsymbol{e}}_{\dot{\boldsymbol{\delta}}}(\boldsymbol{e}_{\dot{\boldsymbol{\delta}}}, \boldsymbol{e}_{\boldsymbol{F}_t}(\boldsymbol{e}_{\boldsymbol{\sigma}}))$ is Lipschitz with respect to $\boldsymbol{e}_{\boldsymbol{\sigma}}$, and we have

$$\|\dot{\boldsymbol{e}}_{\dot{\boldsymbol{\delta}}}(\boldsymbol{e}_{\dot{\boldsymbol{\delta}}}, \boldsymbol{e}_{\boldsymbol{F}_t}(\boldsymbol{e}_{\boldsymbol{\sigma}})) - \dot{\boldsymbol{e}}_{\dot{\boldsymbol{\delta}}}(\boldsymbol{e}_{\dot{\boldsymbol{\delta}}}, \boldsymbol{e}_{\boldsymbol{F}_t}(\boldsymbol{0}))\| \le L_1\|\boldsymbol{e}_{\boldsymbol{\sigma}}\|, \tag{40}$$

where L_1 is a Lipschitz constant. Noticing (38), $\dot{\boldsymbol{e}}_{\boldsymbol{\sigma},\boldsymbol{p}_\sigma}$ is Lipschitz with respect to $\boldsymbol{e}_{\ddot{\boldsymbol{\sigma}}}$. According to (26), (27), and (28), for every bounded F_{td}, $\boldsymbol{e}_{\ddot{\boldsymbol{\sigma}}}$ can be expressed as $\boldsymbol{e}_{\ddot{\boldsymbol{\sigma}}}(e_\phi, e_\theta)$. It is easy to prove that $\boldsymbol{e}_{\ddot{\boldsymbol{\sigma}}}(e_\phi, e_\theta)$ is Lipschitz with respect to $[e_\phi, e_\theta]^\top$. Then, $\dot{\boldsymbol{e}}_{\boldsymbol{\sigma},\boldsymbol{p}_\sigma}(\boldsymbol{e}_{\boldsymbol{\sigma},\boldsymbol{p}_\sigma}, \boldsymbol{e}_{\ddot{\boldsymbol{\sigma}}}(e_\phi, e_\theta))$ is Lipschitz with respect to $[e_\phi, e_\theta]^\top$. Considering the definition of $V_{\boldsymbol{\sigma}}$ in (32) and the boundary of $\boldsymbol{\sigma}$ in (1). Furthermore, V_σ is continuous differentiable, which means it is bounded. Thus,

$$\begin{aligned}&\frac{\partial V_{\boldsymbol{\sigma}}}{\partial \boldsymbol{e}_{\boldsymbol{\sigma},\boldsymbol{p}_\sigma}}[\dot{\boldsymbol{e}}_{\boldsymbol{\sigma},\boldsymbol{p}_\sigma}(\boldsymbol{e}_{\boldsymbol{\sigma},\boldsymbol{p}_\sigma}, \boldsymbol{e}_{\ddot{\boldsymbol{\sigma}}}(e_\phi, e_\theta)) - \dot{\boldsymbol{e}}_{\boldsymbol{\sigma},\boldsymbol{p}_\sigma}(\boldsymbol{e}_{\boldsymbol{\sigma},\boldsymbol{p}_\sigma}, \boldsymbol{e}_{\ddot{\boldsymbol{\sigma}}}(\boldsymbol{0}))] \\ \le& L_2\|[e_\phi, e_\theta]\|,\end{aligned} \tag{41}$$

where L_2 is a positive constant.

Substituting inequalities (40) and (41) into (39), we have

$$\begin{aligned}\dot{V}_t =& -am_p^{-1}\boldsymbol{e}_{\dot{\boldsymbol{\delta}}}\boldsymbol{K}_{\dot{\boldsymbol{\delta}}}\boldsymbol{e}_{\dot{\boldsymbol{\delta}}} + am_p^{-1}L_1\|\boldsymbol{e}_{\dot{\boldsymbol{\delta}}}\|\|\boldsymbol{e}_{\boldsymbol{\sigma}}\| \\ & - b(\boldsymbol{e}_{\boldsymbol{\sigma}}^\top\boldsymbol{K}_{\boldsymbol{\sigma}}\boldsymbol{e}_{\boldsymbol{\sigma}} + \boldsymbol{e}_{\boldsymbol{p}_{\boldsymbol{\sigma}}}^\top\boldsymbol{K}_{\boldsymbol{p}_{\boldsymbol{\sigma}}}\boldsymbol{e}_{\boldsymbol{p}_{\boldsymbol{\sigma}}}) + bL_2\|[e_\phi\ e_\theta]\| \\ & - (\boldsymbol{e}_{\boldsymbol{\eta}}^\top\boldsymbol{K}_{\boldsymbol{\eta}}\boldsymbol{e}_{\boldsymbol{\eta}} + \boldsymbol{e}_{\boldsymbol{p}_{\boldsymbol{\eta}}}^\top\boldsymbol{K}_{\boldsymbol{p}_{\boldsymbol{\eta}}}\boldsymbol{e}_{\boldsymbol{p}_{\boldsymbol{\eta}}})/(\sqrt{2}\|\boldsymbol{e}_{\boldsymbol{\eta},\boldsymbol{p}_{\boldsymbol{\eta}}}\|). \\ \leq& -a\lambda_{\dot{\boldsymbol{\delta}}}\|\boldsymbol{e}_{\dot{\boldsymbol{\delta}}}\|^2 + am_p^{-1}L_1\|\boldsymbol{e}_{\dot{\boldsymbol{\delta}}}\|\|\boldsymbol{e}_{\boldsymbol{\sigma}}\| - b\lambda_{\boldsymbol{\sigma}}\|\boldsymbol{e}_{\boldsymbol{\sigma},\boldsymbol{p}_{\boldsymbol{\sigma}}}\|^2 \\ & + bL_2\|[e_\phi\ e_\theta]\| - \lambda_{\boldsymbol{\eta}}\|\boldsymbol{e}_{\boldsymbol{\eta},\boldsymbol{p}_{\boldsymbol{\eta}}}\|, \end{aligned} \tag{42}$$

where $\lambda_{\boldsymbol{\eta}} = \min\left(\lambda_{min}(\boldsymbol{K}_{\boldsymbol{\eta}}), \lambda_{min}(\boldsymbol{K}_{\boldsymbol{p}_{\boldsymbol{\eta}}})\right)/\sqrt{2}$, $\lambda_{\boldsymbol{\sigma}} = \min\left(\lambda_{min}(\boldsymbol{K}_{\boldsymbol{\sigma}}),\ \lambda_{min}(\boldsymbol{K}_{\boldsymbol{p}_{\boldsymbol{\sigma}}})\right)$, $\lambda_{\dot{\boldsymbol{\delta}}} = \lambda_{min}(\boldsymbol{K}_{\dot{\boldsymbol{\delta}}})/m_p^{-1}$, where $\lambda_{min}(\cdot)$ denotes the minimum eigenvalue of a matrix.

According to the definitions (19), (19), (21), and (21), $\|\boldsymbol{e}_{\boldsymbol{\sigma}}\| \leq \|\boldsymbol{e}_{\boldsymbol{\sigma},\boldsymbol{p}_{\boldsymbol{\sigma}}}\|$ and $\|[e_\phi\ e_\theta]\| \leq \|\boldsymbol{e}_{\boldsymbol{\eta},\boldsymbol{p}_{\boldsymbol{\eta}}}\|$. Then,

$$\begin{aligned}\dot{V}_t \leq& -a\lambda_{\dot{\boldsymbol{\delta}}}\|\boldsymbol{e}_{\dot{\boldsymbol{\delta}}}\|^2 + am_p^{-1}L_1\|\boldsymbol{e}_{\dot{\boldsymbol{\delta}}}\|\|\boldsymbol{e}_{\boldsymbol{\sigma}}\| - b\lambda_{\boldsymbol{\sigma}}\|\boldsymbol{e}_{\boldsymbol{\sigma},\boldsymbol{p}_{\boldsymbol{\sigma}}}\|^2 \\ & + bL_2\|[e_\phi\ e_\theta]\| - \lambda_{\boldsymbol{\eta}}\|\boldsymbol{e}_{\boldsymbol{\eta},\boldsymbol{p}_{\boldsymbol{\eta}}}\| \\ =& -\begin{bmatrix} a\|\boldsymbol{e}_{\dot{\boldsymbol{\delta}}}\|/\sqrt{2} \\ b\|\boldsymbol{e}_{\boldsymbol{\sigma},\boldsymbol{p}_{\boldsymbol{\sigma}}}\|/\sqrt{2}\end{bmatrix}^\top \begin{bmatrix} 2\lambda_{\dot{\boldsymbol{\delta}}} & -\frac{\sqrt{a}L_1}{\sqrt{b}m_p} \\ -\frac{\sqrt{a}L_1}{\sqrt{b}m_p} & 2\lambda_{\boldsymbol{\sigma}}\end{bmatrix} \begin{bmatrix} a\|\boldsymbol{e}_{\dot{\boldsymbol{\delta}}}\|/\sqrt{2} \\ b\|\boldsymbol{e}_{\boldsymbol{\sigma},\boldsymbol{p}_{\boldsymbol{\sigma}}}\|/\sqrt{2}\end{bmatrix} \\ & +(bL_2 - \lambda_{\boldsymbol{\eta}})\|\boldsymbol{e}_{\boldsymbol{\eta},\boldsymbol{p}_{\boldsymbol{\eta}}}\|. \end{aligned} \tag{43}$$

Noticing the upper bound of b in (33), the upper bound of the second term on the right hand of (43) is

$$(bL_2 - \lambda_{\boldsymbol{\eta}})\|\boldsymbol{e}_{\boldsymbol{\eta},\boldsymbol{p}_{\boldsymbol{\eta}}}\| < 0.$$

Defining $\boldsymbol{Q} = \begin{bmatrix} 2\lambda_{\dot{\boldsymbol{\delta}}} & -(\sqrt{a}L_1)/(\sqrt{b}m_p) \\ -(\sqrt{a}L_1)/(\sqrt{b}m_p) & 2\lambda_{\boldsymbol{\sigma}}\end{bmatrix}$.
Noticing the upper bound of a in (33), $\boldsymbol{Q}$ is positive definite, then

$$\begin{aligned}& -\begin{bmatrix} a\|\boldsymbol{e}_{\dot{\boldsymbol{\delta}}}\|/\sqrt{2} \\ b\|\boldsymbol{e}_{\boldsymbol{\sigma},\boldsymbol{p}_{\boldsymbol{\sigma}}}\|/\sqrt{2}\end{bmatrix}^\top \boldsymbol{Q} \begin{bmatrix} a\|\boldsymbol{e}_{\dot{\boldsymbol{\delta}}}\|/\sqrt{2} \\ b\|\boldsymbol{e}_{\boldsymbol{\sigma},\boldsymbol{p}_{\boldsymbol{\sigma}}}\|/\sqrt{2}\end{bmatrix} \\ \leq& -\lambda_{min}(\boldsymbol{Q})(a\|\boldsymbol{e}_{\dot{\boldsymbol{\delta}}}\|^2/2 + b\|\boldsymbol{e}_{\boldsymbol{\sigma},\boldsymbol{p}_{\boldsymbol{\sigma}}}\|^2/2) < 0. \end{aligned} \tag{44}$$

Therefore, $\dot{V}_t$ is negative definite. Substituting (44) into (43), we have

$$\begin{aligned}\dot{V}_t \leq& -\lambda_{min}(\boldsymbol{Q})(a\|\boldsymbol{e}_{\dot{\boldsymbol{\delta}}}\|^2/2 + b\|\boldsymbol{e}_{\boldsymbol{\sigma},\boldsymbol{p}_{\boldsymbol{\sigma}}}\|^2/2) \\ & + (bL_2 - \lambda_{\boldsymbol{\eta}})\|\boldsymbol{e}_{\boldsymbol{\eta},\boldsymbol{p}_{\boldsymbol{\eta}}}\|. \end{aligned} \tag{45}$$

Recalling (32), Let $\lambda = \min\left(\lambda_{min}(\boldsymbol{Q})/\sqrt{2}, \lambda_{\boldsymbol{\eta}} - bL_2\right)$, then, the time derivative of Lyapunov candidate V_t is bounded by

$$\dot{V}_t \leq -\lambda\left(\frac{a}{2}\|\boldsymbol{e}_{\dot{\boldsymbol{\delta}}}\|^2 + \frac{b}{2}\|\boldsymbol{e}_{\boldsymbol{\sigma},\boldsymbol{p}_{\boldsymbol{\sigma}}}\|^2 + \frac{\sqrt{2}}{2}\|\boldsymbol{e}_{\boldsymbol{\eta},\boldsymbol{p}_{\boldsymbol{\eta}}}\|\right) = -\lambda V_t.$$

Consequently, the zero equilibrium of the errors $\boldsymbol{e}_{\dot{\boldsymbol{\delta}}}$, $\boldsymbol{e}_{\boldsymbol{\sigma},\boldsymbol{p}_{\boldsymbol{\sigma}}}$ and $\boldsymbol{e}_{\boldsymbol{\eta},\boldsymbol{p}_{\boldsymbol{\eta}}}$ are exponentially stable.

3. SIMULATION

In this section, simulations are carried out to show the feasibility and effectiveness of the proposed controller and model in the SimMechianics environment.

3.1 QSL Parameters

The model parameters are listed in Table 1. The drag coefficients, including drag force coefficients $\boldsymbol{D}_\xi$, $\boldsymbol{D}_\delta$ and drag torque coefficients $\boldsymbol{D}_\eta$, are taken into consideration and obtained by the method in Modirrousta and Khodabandeh (2015). The values of the drag coefficients are

Table 1. Physical Parameters

	Value	Unit		Value	Unit
g	9.807	m/s^2	I_{qxx}	12.71×10^{-3}	$kg\cdot m^2$
m_q	1.331	kg	I_{qyy}	12.71×10^{-3}	$kg\cdot m^2$
m_p	0.063	kg	I_{qzz}	2.37×10^{-2}	$kg\cdot m^2$
l_r	0.225	m	I_{pxx}	3.4×10^{-5}	$kg\cdot m^2$
l	0.505	m	I_{pyy}	3.4×10^{-5}	$kg\cdot m^2$
c_t	1.6×10^{-5}	$N/(rad/s)^2$	I_{pzz}	6.7×10^{-5}	$kg\cdot m^2$
c_q	5×10^{-7}	$N/(rad/s)^2$			

$D_{qx} = D_{qy} = D_{qz} = 0.2$, $D_{px} = D_{py} = D_{pz} = 0.08$, $D_\phi = D_\theta = D_\psi = 0.1$. The values of the control parameters are $k_1 = k_2 = 0.2$, $k_3 = k_4 = k_5 = 0.1$, $k_6 = 0.005$, $k_7 = k_8 = k_9 = k_{10} = 6$, $k_{11} = k_{12} = 0.5$, $k_{13} = 3$, $\rho_m = 5$, $\rho_o = 40$.

3.2 SIL Simulation Results

In this subsection, two simulation cases are given. The first one is about the middle-loop swing angle sub-controller for the load; the second one is about the outer-loop velocity sub-controller for the load. For comparison, we simulate the other PID controllers in the first two cases to verify the effectiveness of the proposed nonlinear cascade controller. The parameters of the PID controllers are obtained by Wang et al. (2000) to reduce the accumulative errors in the simulations.

In the first simulation case, as shown in Fig. 3, the load tracks the desired swing angles α_d and β_d from $[0\ 0]^\top(deg)$. It is find that the settling time of designed middle-loop sub-controller is shorter than PID controller.

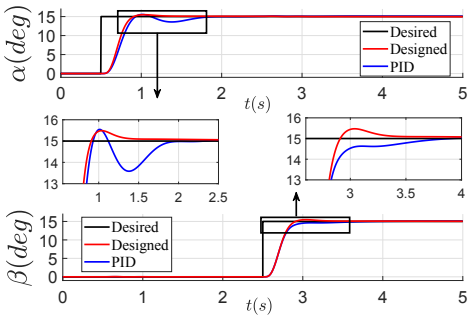

Fig. 3. Simulation results of middle-loop swing angle control for the load.

The second case simulates that the load of the QSL tracks the desired velocities, as shown in Fig. 4. The settling time of the proposed controller is much less than the PID controller. Due to the coupling disturbance, the performance of both controller step inputs inevitably slides down. However, the performance of the designed controller is much better than the PID controller, especially at $3s$, $5s$, and $8s$.

Moreover, in order to make quantitative comparisons of the simulation results obtained by the designed nonlinear controllers and PID controllers, some performance indexes for the first step response of those simulations are computed and presented in Table 2.

An additional simulation case is given, the proposed controller, combined with a normal PID position sub-controller, is implemented and tested in a complete simulation task. A three-dimensional simulation is presented in Fig. 5, and an animation is accompanied: `https://youtu.be/4T-D0rYhc8I`. The results shows that the QSL can realize accurate trajectory tracking by the proposed nonlinear cascade controller.

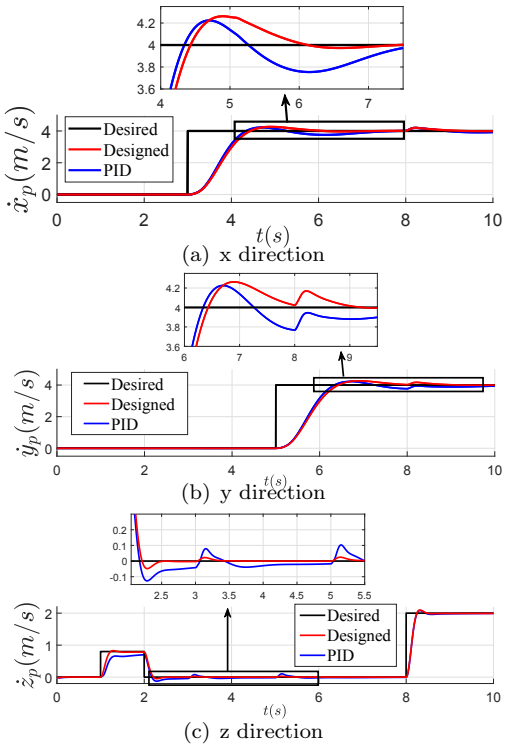

Fig. 4. Simulation results of outer-loop velocity control.

Table 2. Comparison of simulation results between designed controller and PID controller

	Rise time(s)	Max overshoot	Settling time(s)	Rise time(s)	Max overshoot	Settling time(s)
	Designed			PID		
α	**2.1**	**3.04%**	**0.36**	0.24	3.62%	1.1
β	**2.1**	**3.1%**	**0.37**	0.24	3.63%	1.12
$\dot{x}_p$	0.85	**6.5%**	**2.2**	0.79	5.6%	3.58
$\dot{y}_p$	0.86	**6.4%**	**2.18**	0.77	.7%	3.57
$\dot{z}_p$	**1.6**	**3.47%**	**0.22**	0.16	4.1%	0.23

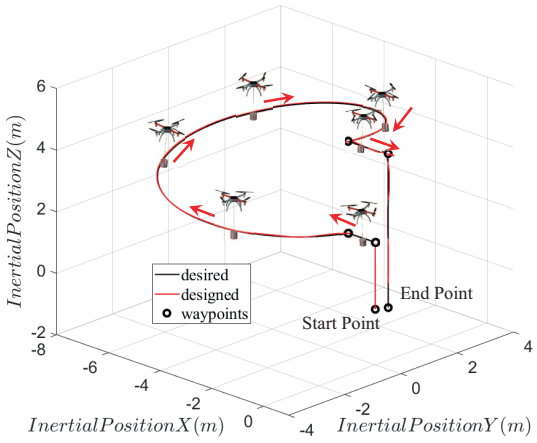

Fig. 5. Simulation results of trajectory tracking.

To sum up, good results were obtained from our simulations, which implies that the designed controller can realize active velocity control for the load and has better control performance compared to the existing PID controller.

4. CONCLUSIONS

In this paper, a new dynamical model that considers the air resistance is proposed by Lagrangian approach. Based on the model, a novel nonlinear cascade controller is proposed to realize accurate and stable velocity control for the load of the QSL, and the exponential stability of the entire system is proved. Simulations in SimMechianics demonstrate the validity and performance of the dynamical model and the control design.

REFERENCES

Arnol'd, V.I. (2013). *Mathematical methods of classical mechanics*, volume 60. Springer Science & Business Media.

Choi, Y.C. and Ahn, H.S. (2015). Nonlinear control of quadrotor for point tracking: Actual implementation and experimental tests. *IEEE/ASME transactions on mechatronics*, 20(3), 1179–1192.

Davis, E. and Pounds, P.E. (2017). Direct sensing of thrust and velocity for a quadrotor rotor array. *IEEE Robotics and Automation Letters*, 2(3), 1360–1366.

Goodarzi, F.A., Lee, D., and Lee, T. (2015). Geometric control of a quadrotor UAV transporting a payload connected via flexible cable. *International Journal of Control, Automation and Systems*, 13(6), 1486–1498.

Guerrero, M., Mercado, D., Lozano, R., and García, C. (2015a). IDA-PBC methodology for a quadrotor UAV transporting a cable-suspended payload. In *Unmanned Aircraft Systems (ICUAS), 2015 International Conference on*, 470–476. IEEE.

Guerrero, M., Mercado, D., Lozano, R., and García, C. (2015b). Passivity based control for a quadrotor UAV transporting a cable-suspended payload with minimum swing. In *Decision and Control (CDC), 2015 IEEE 54th Annual Conference on*, 6718–6723. IEEE.

Modirrousta, A. and Khodabandeh, M. (2015). A novel nonlinear hybrid controller design for an uncertain quadrotor with disturbances. *Aerospace Science and Technology*, 45, 294–308.

Palunko, I., Cruz, P., and Fierro, R. (2012). Agile load transportation: Safe and efficient load manipulation with aerial robots. *IEEE robotics & automation magazine*, 19(3), 69–79.

Qian, L. and Liu, H.H. (2019). Path following control of a quadrotor UAV with a cable suspended payload under wind disturbances. *IEEE Transactions on Industrial Electronics*. DOI: 10.1109/TIE.2019.2905811.

Raffo, G.V. and de Almeida, M.M. (2016). Nonlinear robust control of a quadrotor UAV for load transportation with swing improvement. In *2016 American Control Conference (ACC)*, 3156–3162. IEEE.

Sreenath, K., Lee, T., and Kumar, V. (2013). Geometric control and differential flatness of a quadrotor UAV with a cable-suspended load. In *CDC*, 2269–2274. Citeseer.

Wang, W., Zhang, J.T., and Chai, T.Y. (2000). A survey of advanced pid parameter tuning methods. *ACTA AUTOMATICA SINICA*, 26(3), 347–355.

Wu, Y., Hu, K., and Sun, X.M. (2018a). Modeling and control design for quadrotors: A controlled Hamiltonian systems approach. *IEEE Transactions on Vehicular Technology*, 67(12), 11365–11376.

Wu, Y., Lv, Z., and Yu, X. (2018b). Modeling and passivity analysis by hamiltonian approach for a quadrotor transporting a cable-suspended payload. In *2018 57th Annual Conference of the Society of Instrument and Control Engineers of Japan (SICE)*, 529–532. IEEE.